ACS APPLIED MATERIALS & INTERFACES

Article

Fast Crystallization and improved Stability of Perovskite Solar Cells with ZnSnO Electron Transporting Layer: Interface Matters

Ashok Bera, Arif D. Sheikh, Md Azimul Haque, Riya Bose, Erkki Alarousu, Omar F. Mohammed, and Tom Wu

ACS Appl. Mater. Interfaces, **Just Accepted Manuscript** • DOI: 10.1021/acsami.5b09182 • Publication Date (Web): 03 Dec 2015

ACS Publications

ACS Applied Materials & Interfaces is published by the American Chemical Society.
1155 Sixteenth Street N.W., Washington, DC 20036

Fast Crystallization and improved Stability of Perovskite Solar Cells with Zn_2SnO_4 Electron Transporting Layer: Interface Matters

Ashok Bera[†], *Arif D. Sheikh*[†], *Md. Azimul Haque*[†], *Riya Bose*[‖], *Erkki Alarousu*[‖], *Omar F. Mohammed*[‖], *Tom Wu*[†]*

[†]Materials Science and Engineering, King Abdullah University of Science and Technology (KAUST), Thuwal, 23955-6900, Saudi Arabia.
E-mail: tao.wu@kaust.edu.sa

[‖]Solar and Photovoltaics Engineering Research Center, Division of Physical Science and Engineering, King Abdullah University of Science and Technology (KAUST), Thuwal, 23955-6900, Saudi Arabia

Abstract

Here we report that mesoporous ternary oxide Zn_2SnO_4 can significantly promotes the crystallization of hybrid perovskite layers and serves as an efficient electron transporting material in perovskite solar cells. Such devices exhibit an energy conversion efficiency of 13.34%, which is even higher than that achieved with the commonly used TiO_2 in the similar experimental conditions (9.1%). Simple one-step spin coating of $CH_3NH_3PbI_{3-x}Cl_x$ on Zn_2SnO_4 is found to lead to rapidly crystalized bilayer perovskite structure without any solvent engineering. Furthermore, ultrafast transient absorption measurement reveals efficient charge transfer at the Zn_2SnO_4/perovskite interface. Most importantly, solar cells with Zn_2SnO_4 as the electron-transporting material exhibit negligible electrical hysteresis and exceptionally high stability without encapsulation for over one month. Besides underscoring Zn_2SnO_4 as a highly promising electron transporting material for perovskite solar cells, our results demonstrate the significant role of interfaces on improving the perovskite crystallization and photovoltaic performance.

Keywords: perovskite solar cells; Zn_2SnO_4; electron transport layer; transient absorption spectroscopy

1. Introduction

Organometallic hybrid perovskites have recently attracted enormous attention for applications in thin film photovoltaic technology.[1-16] These hybrid methylammonium lead halide perovskites (e.g., $CH_3NH_3PbX_3$, X= I, Cl, Br) exhibit superior properties such as solution processability,[3, 13] strong light absorption,[17] ambipolar charge transport,[5, 18] long carrier diffusion length,[6, 19] and tunable chemical composition and band gap.[10, 20-21] In commonly used perovskite solar cell structures, a layer of perovskite absorber is deposited over a compact or mesoporous (mp) oxide electron transport layer (ETL), which is followed by a hole transporting layer (HTL) made of typically 2,2',7,7'-tetrakis-(N,N-di-p-methoxyphenylamine)-9,9'-spirobifluorene (spiro-MeOTAD). Despite the escalating efficiency, the bottleneck for the perovskite-based photovoltaic technology is the tendency of device degradation by humidity due to the hygroscopic nature of the organic ions in hybrid perovskites. Furthermore, in the solution-based process, the crystallization of the perovskite layers is critical but complex to precisely control, which unfortunately compromises the performance of the final solar cells.

It is a consensus that the perovskite crystallization closely depends on multiple factors such as solvent choice, solution concentration, precursor composition, and deposition temperature.[3, 22-24] For the commonly used ETL of mp-TiO_2, there have been significant discrepancies in the literature as a result of the poor control on the crystallization process and the resultant morphology of the perovskite layers, and the solar cell performance often suffer from the incomplete coverage of the perovskite layer.[25-26] Compromised growth control and defective perovskite/ETL interface also contribute to severe hysteresis observed in the electrical characterizations.[3] Therefore, a satisfactory ETL should not only lower the dark current and series resistance,[27] but also promote the crystallization of high-quality perovskite layers. So far,

most reports in literature were focused on improving the quality of perovskite films formed on mp-TiO_2, which remains as the dominant ETL. However, finding alternative oxide ETL with appropriate band alignments, high electron mobility and solution processability clearly represents a powerful but largely unexplored route toward realizing high-performance perovskite solar cells.

In this paper, we report the superior performance of ternary oxide Zn_2SnO_4 (ZTO) as ETL in mixed-halide perovskite ($CH_3NH_3PbI_{3-x}Cl_x$) solar cells. ZTO was previously explored as electron transporter in solar cells,[28-32] but its advantages as an effective template for growing high-quality perovskite layers deserve in-depth explorations. In our work, we found that interfacing with mp-ZTO could significantly improve the crystallization of $CH_3NH_3PbI_{3-x}Cl_x$ layer in the single-step spin coating process. The rate of perovskite crystallization on mp-ZTO is much faster than that on mp-TiO_2, which promotes the formation of bilayer perovskite structures with a uniformly crystallized overlayer and perovskite grains are as large as 2 μm. The energy conversion efficiency of the perovskite solar cells with the ZTO ETL reaches 13.34%, which is even higher than that reported for devices with one-step spin-coated $CH_3NH_3PbI_{3-x}Cl_x$ on TiO_2 ETL.[13, 25, 33-37] Furthermore, the perovskite solar cells with ZTO as ETL exhibit negligible electrical hysteresis and high stability without encapsulation, which underscore the significant role of ZTO/perovskite interface on improving the overall device performance.

2. Experimental section

2.1. Materials preparation

Methylammonium iodide (CH_3NH_3I) was synthesized following the previously reported method.[13] 2.7M CH_3NH_3I and 0.9M $PbCl_2$ was dissolved in anhydrous N,N-

Dimethylformamide, to produce a mixed halide perovskite precursor solution. ZTO nanoparticles are synthesized by decomposing a mixture of zinc and tin tert-butylamine complexes under hydrothermal conditions.[29] ZTO paste was prepared using the procedure similar to a previous report on making the TiO_2 paste.[9] First, ZTO nanoparticles were dispersed in ethanol followed by adding Ethylcellulose, Lauric acid, and Terpineol, and then ethanol was removed from the solution using a rotary evaporator to obtain viscous pastes. Finally, the paste was diluted with ethanol in 3:2 weight ratio for the spin coating.

2.2. Solar cell fabrication

Fluorine-doped tin oxide ($F:SnO_2$) coated glass (Pilkington TEC A7) was etched with Zn powder and 2 M HCl and then washed in DI water. The etched substrate was then cleaned by detergent, DI water, acetone and ethanol using an ultrasonic cleaner, and then dried. The substrate underwent an oxygen plasma treatment for 10 minutes prior to the deposition of compact ZTO hole blocking layer. Compact ZTO was deposited by spin coating a solution of Zinc acetate and Tin acetate in 2-methoxy ethanol in 2:1 molar ratio for 40 seconds at 3000 rpm. Ethanolamine was used as the stabilizer.[38] Then the coated thin film was dried at 150 °C for 15 min followed by an annealing at 500°C for 30 min. The mp-ZTO was deposited by spin coating the diluted paste for 45 seconds at 2000 rpm and then annealed at 500 °C for 1 hour. The perovskite precursor solution was then spin coated on mp-electrode at 2000 rpm for 60 seconds and dried at 100°C for about 1 hour. A 68 mM Spiro-OMeTAD solution in chlorobenzene containing 55 mM tert-butylpyridine and 9 mM lithium bis(trifluoromethylsyfonyl)imide (LiTFSI) salt was spun on the perovskite-coated substrates at a rate of 2000 rpm for 45 seconds and then the cells were kept in the dark for overnight. Finally, Au electrodes with a thickness of 70 nm were evaporated by thermal evaporation to complete the device.

2.3. Materials characterizations

The structure and the morphology of the $CH_3NH_3PbI_{3-x}Cl_x$ grown on mp-ZTO were examined suing X-ray diffractometer (Bruker D8) and field emission scanning electron microscopy (FEI-NANO NOVA-600) and atomic force microscopy (Bruker Dimension Icon). The porosity and the surface area of the mesoporous layers were measured via the Brunauer-Emmett-Teller (BET) method on a Micromeritics ASAP 2420 system. The absorption spectra were measured using a Varian carry 6000i spectrophotometer.

2.4. Solar cell characterizations

The current density–voltage (*J–V*) curves were measured using Oriel PVIV test solution software connected with a source meter (Keithley 2400) under the illumination at 100 mW/ cm^2 illumination (AM 1.5G) from a solar simulator (Newport, Oriel Class A, 91195A) and a calibrated Si-reference cell certificated by NREL. The *J–V* curves of all devices were measured by masking the unwanted area with black tape so that the exposed active area was 0.2 cm^2. To characterize the device stability, we stored the samples in dry air in a desiccator between the measurements. The external quantum efficiency of the device was measured using an Oriel IQE-200 quantum efficiency measurement system.

3. Result and discussion

Figure 1(a) illustrates the cubic-type spinel structure of the ZTO. Figure 1(b) shows the schematic band alignment of the ZTO ETL, perovskite $CH_3NH_3PbI_{3-x}Cl_x$ absorber and spiro-MeOTAD HTL, where the energy bands are well aligned for the effective separation and injection of photo-excited carriers. Spinel-structured ZTO has a band gap of 3.7 eV, much wider than that of TiO_2 (3.2 eV), and its conduction band edge is about 0.1 eV lower than that of TiO_2.[39] One main advantage of using ZTO as ETL is that its electron mobility is on the order of

10-15 $cm^2V^{-1}S^{-1}$,[40-41] much higher than that of TiO_2 (0.1−4 cm^2 V^{-1} s^{-1}).[42] In dye sensitized solar cells (DSSC), it has been recently reported that the charge injection from the sensitizer and the electron diffusion through the nanoparticle network are significantly faster for the ZTO photoanode than the TiO_2-based counterpart.[43] Furthermore, ZTO thin films with high electron mobility can be formed below 500 °C by solution processing.[38] In contrast, other ternary oxides often need much higher temperatures to crystalize, e.g., formation of high-quality perovskite oxide $SrTiO_3$ layers occurs at about 750 °C. [44]

The X-ray diffraction (XRD) spectrum of the mp-ZTO layer formed after annealing at 500 °C is shown in Figure 1(c), which confirms the well-crystalized cubic spinal phase (JCPDS no. 24-1470). The average pore diameter of mp-ZTO is 16.4 nm, and its surface area is 63.4 m^2/g, as estimated from the BET measurement (supporting information Figure S1a). These values are comparable to those of the mp-TiO_2 photoelectrode (pore diameter: 23 nm; surface area: 69 m^2/g) obtained from the commercial TiO_2 paste.[45] Because ZTO and FTO have very similar refractive indices, coating the ZTO photoelectrode on FTO-coated glass substrates does not change much the transmittance spectra (supporting information Figure S1b).[43]

In this work, we deposited $CH_3NH_3PbI_{3-x}Cl_x$ perovskite layer via one-step spin coating onto the FTO/cp-ZTO/mp-ZTO substrates. Perovskite layers can also be deposited via two-step sequential deposition process, i.e., a PbI_2 layer was spin-coated first on mp-ZTO, followed by dipping the substrate in CH_3NH_3I (MAI) solution.[30] But such a two-step process was found to lead to poor morphology and incomplete surface coverage of the perosvskite layers, and the fabricated perovskite solar cells with ZTO ETL exhibited an efficiency of merely 7%.[30] In our experiments, a solution of $PbCl_2$ and MAI in dimethylforamide (DMF) with a molar ratio of 1:3 was spin-coated on the substrates and annealed at 100 °C.

The transformation of the perovskite phase was characterized by XRD and transmittance measurements. Figure 2a shows the time-dependent evolution of the XRD patterns of the as-prepared $CH_3NH_3PbI_{3-x}Cl_x$ film on FTO/cp-ZTO/mp-ZTO. Surprisingly, after annealing for only one minute, the perovskite film already displayed intense characteristic peaks. Sharp peaks at 14.2°, 28.5°, 31.87° and 43.2° correspond to the (110), (220), (310) and (330) planes of $CH_3NH_3PbI_{3-x}Cl_x$, respectively, and other weaker peaks can be assigned to (112), (022) and (224) planes, indicating the formation of perovskite phase with high crystallinity.[46-47] The complete transformation into the perovskite phase was observed within 10 minutes of annealing. This fast crystallization was also confirmed by the optical transmittance measurements; as shown in Figure 2b, the characteristics absorption reached saturation after 10 minutes of annealing. In contrast, for mp-TiO_2, the transmittance spectra continuously evolved for the first 30 min, and the formation of perovskite was completed only after annealing of one hour (supporting information Figure S2). This agrees with the reported annealing times of 45 min at 100 °C necessary to prepare high-quality $CH_3NH_3PbI_{3-x}Cl_x$ layers on TiO_2 ETL.[48] Our results indicate that mp-ZTO effectively accelerates the crystallization of the perovskite layer, which was further confirmed by the photos taken during the annealing process (supporting information Figure S3). The color of the $CH_3NH_3PbI_{3-x}Cl_x$ film on mp-TiO_2 remained yellow even after 30 min of annealing, and it needed about one hour to complete the formation of perovskite phase,[4, 49] whereas the $CH_3NH_3PbI_{3-x}Cl_x$ film on mp-ZTO became dark brown in the very first minute. This intriguing behavior of fast crystallization of perovskite on mp-ZTO could be related to the efficient nucleation of perovskite grains at the perovskite/ETL interface, which warrants further studies. The transmittance spectra of mp-ZTO and mp-TiO_2 photoanodes (inset of figure 2b) in

the UV-to-near-visible range show that mp-ZTO transmits more light compared to mp-TiO_2, which benefits the effective light absorption of the perovskite layers.

Morphology of the perovskite layers was investigated using atomic force microscopy (AFM) and scanning electron microscopy (SEM). The film surface is featured with grains as large as two μm (Figure 3a), and the root-mean-square roughness is 27.2 nm with the scanning area of 5μm × 5μm. The top-view SEM image in Figure 3b confirms that the entire film is composed of homogeneous, well-crystallized perovskite grains. In contrast, single-step spin coating on the mp-TiO_2 layer led to non-uniform perovskite islands with incomplete surface coverage, as shown in supporting information Figure S4. In addition, the cross-sectional SEM image of the optimized device shows a uniform bilayer structure (Figure 3c), i.e., the perovskite is completely infiltrated into the pores of the mp-ZTO film, and also forms a uniform well-crystallized perovskite overlayer about 200 nm thick with full surface coverage. This kind of bi-layer perovskite morphology on ETL benefits the solar cell performance, which was previously achieved only when solvent engineering was applied to the spin coating process.[3]

The photovoltaic performance of these $CH_3NH_3PbI_{3-x}Cl_x$ solar cells was measured in air under AM 1.5G (100 mW/cm^2) simulated solar irradiation. The *J–V* characteristics of the champion device with the ZTO ETL measured in dark and under light are given in Figure 4a. Short-circuit photocurrent density (J_{SC}) of 19.58mA/cm^2, open-circuit voltage (V_{OC}) of 0.932V, and fill factor (FF) of 72.65% were observed, leading to PCE (η) of 13.34 % . This efficiency is higher than those of recently reported perovskite solar cells with one-step spin-coated $CH_3NH_3PbI_{3-x}Cl_x$ layers on mp-TiO_2 ETL.[13, 25, 33-37] The external quantum efficiency (EQE) of our $CH_3NH_3PbI_{3-x}Cl_x$ solar cells was measured by monitoring the photocurrent at different wavelengths, and the data is shown in Figure 4b. The estimated current density by integrating the

EQE spectrum with the AM 1.5G solar spectrum matches well with J_{SC}, confirming the validity of our measurements. The statistics of 24 perovskite solar cells using mp-ZTO ETL indicate consistent performance, as shown in Supporting Information, Figures S5. Our devices have an average PCE of 12.42% with J_{SC} of 19.86 mA/cm^2, V_{OC} of 0.92 V, and FF of 68%. V_{OC} of the ZTO-based solar cells is slightly lower than that of the TiO_2-based ones,[26] which could result from the slightly lower conduction band edge of ZTO compared to TiO_2.

We should note here special attentions are needed for the preparation of the ZTO layers, which is the key to achieving high efficiency in the perovskite solar cells. In particular, to prepare the ZTO layers, we spin coated a solution of zinc acetate and tin acetate in 2-methoxy ethanol with ethanolamine as a stabilizer.[38] In contrast, if we simply used zinc chloride and tin chloride in alcohol,[30] we found significant phase separation into ZnO and SnO, and the maximum efficiency achieved in the devices was only about 5%. Furthermore, we found that using ZTO as both the compact layer and the mp-layer is critical for achieving efficient perovskite solar cells. As control devices, we also tried to combine compact TiO_2 layers and mp-ZTO, but the best performing device showed a PCE of only about 7% (supporting information Figure S6).

Although one-step spin coating of perovskite layers saves processing time compared to the two-step counterpart, such perovskite solar cells in both mesoporous and planar configurations suffer from anomalous hysteresis in the *J-V* characteristics,[3, 34, 50-51] making it difficult to accurately benchmark the device performance. Voltage scanning direction and rate as well as bias history were all found to significantly influence the electrical hysteresis,[34] which could lead to either over or underestimated efficiency values. Structural defects and ferroelectric polarization were hypothesized as the origins of the I−V hysteresis.[34] If the perovskite absorbers

have lots of defects, then the associated interface states could act as traps for electrons and holes. On the other hand, the interface trap states are reduced in perovskite layers with large well-crystalized grains, and high-quality mesoporous ETL also facilitates the quick dissipation of capacitive charges, reducing hysteresis in perovskite solar cells.[50] Since the perovskite layers are well crystallized in our devices, we expect better perovskite/ZTO interfaces and less hysteresis in our device characteristics. Indeed, as shown in Figure 4c, *J-V* curves of our devices exhibited negligible dependence on the scanning directions and rate. For this particular device, the PEC values are 12.6% and 12.4% for reverse ($V_{OC} \rightarrow J_{SC}$) and forward ($J_{SC} \rightarrow V_{OC}$) scanning directions, respectively. In contrast, inset of Figure 4d shows the typical *J–V* characteristics of the perovskite solar cell using mp-TiO_2 as ETL, which shows a significant hysteresis with efficiencies of 9.1% and 7.76% for reverse and forward scanning directions, respectively. The scan rate dependence of the *J-V* characteristics in the ZTO-based device is given in Figure 4d, and no significant change in the *J-V* characteristics was observed up to a scan speed of 0.5 V/s.

Because transient absorption (TA) spectroscopy gives direct information regarding carrier dynamics and excited-state deactivation pathways including electron injection,[52-53] we utilized this method to examine the electron transfer from $CH_3NH_3PbI_{3-x}Cl_x$ to ETL upon photoexcitation. The details of experimental setups can be found in our previous reports.[54-55] The TA data of bilayers of $CH_3NH_3PbI_{3-x}Cl_x$ with ZTO and TiO_2 at the 440 nm excitation are given in Figure 5. The characteristic decay time constant of $CH_3NH_3PbI_{3-x}Cl_x$ with ZTO is estimated to be 0.5 ns (for 90% of the total amplitude). This characteristic decay time is much shorter than those of $CH_3NH_3PbI_{3-x}Cl_x$ with TiO_2 (3.7 ns) and with perovskite ternary oxide $SrTiO_3$ (2.7 ns) [45], which suggest that the extraction of photoelectrons by ZTO is more efficient than the other two oxides.

Stability of perovskite solar cells has been a top concern as a result of the hygroscopic nature of the alkylammonium cation present in the perovskite unit cell. To determine the stability of our devices, we measured *J*sc under constant 100 mW/cm^2 AM 1.5G illumination. We found that after two hours of illumination, J_{SC} of the ZTO-based device decreased by only 12% (Figure 6a), while the TiO_2-based counterpart suffered from a severe J_{SC} decrease of 27%, which is similar to the previous reports.[2, 56] We also monitored the *J-V* characteristics of our devices under dark storage, and the device maintained an efficiency of about 9.8% after one month. The evolution of solar cell parameters is given in Figure 6b, and the *J-V* characteristics after different dark storage times can be found in Supporting Information Figure S7. The average performance of multiple devices after one month of dark storage is given in the supporting information table S1. Recently, we have reported the effects of dark storage in different atmospheres on the commonly studied TiO_2-based perovskite solar cells, and the efficiency generally decreased by more than 50% from its maximum value after 10 days.[36] In the case of ZTO-based devices, we found that the efficiency slightly increased during the first three days, which could be related to the enhanced in p-type conductivity in the LiTFSI-doped spiro-MeOTAD after storage in dry air.[57] The decrease of device efficiency afterwards can be attributed to the sharp decline of J_{SC}. Interestingly, V_{OC} and FF slightly increase with the storage time, which helps to maintain the efficiency at approximately 9.87% even after one month. Recently, Wang et al. proposed that exposure to light lowers the Fermi level of spiro-MeOTAD,[58] which may contribute to the notable increases of V_{OC} and FF during measurements.

The mechanism behind the high stability of perovskite solar cells with ZTO ETL is related to the optimal morphology of perovskite layers. As shown in Figure 3c, the perovskite layers are featured with a well-crystallized overlayer with grains as large as two μm. It is known

that grain boundaries and structural defects are the sites susceptible to the attack of moisture.[59-60] Such optimal crystallization and morphology of the perovskite layers also contributed to the high energy conversion efficiency (Figure 4a) and negligible electrical hysteresis (Figure 4C). Although the structural and chemical properties of the perovskite/ETL interface are difficult to directly probe because of the delicate nature of hybrid perovskites, we might hypothesize that the interfacial bonding between the perovskite and the ZTO layers is quite strong, which suppresses the infiltration of water molecules and improves the device stability.

Our result differs from the previous reports on perovskite solar cells using ZTO as ETL in terms of both synthesis and device performance.[30-32] We deposited the perovskite layers using the simple one-step spin coating method and our experiments revealed the fast crystallization behavior of the perovskite layers on ZTO. The efficiency of our ZTO-based devices is quite high (13.4%) and our devices are almost hysteresis free. Furthermore, there has been no discussion regarding the device stability in the previous reports, whereas our devices remained stable in air with efficiency about 10% for over one month. These merits of using ZTO as ETL in perovskite solar cells would motivate more research works and facilitate the commercialization of perovskite solar cells.

Interface engineering has been identified as the key to achieve high energy conversion efficiency in perovskite solar cells.[4] Proper band alignment is known to facilitate the charge extraction and collection, which guides the selection of ETL during the design of perovskite solar cells. What remains largely unexplored is the role of interface on the nucleation and growth during the solution processing of perovskite. In the present work, we found that ZTO can significantly speed up the crystallization of hybrid perovskite layers, shortening the annealing time from one hour to several minutes. Interestingly, Zn-containing compounds generally appear

to be effective to accelerate the crystallization of perovskite layers. Faster growth of perovskite layers on ZnO ETL by sequential deposition has also been reported recently.[61] There could be at least two reasons behind the fast crystallization of perovskite layers on such Zn-containing ETLs. One may have a thermodynamic origin: the interface energy between perovskites and such ETLs could be small, which favors the nucleation of perovskite grains on the Zn-containing oxides. The other reason may be related to the reaction kinetics. It was recently proposed that the crystallization of $CH_3NH_3PbI_{3-x}Cl_x$ from CH_3NH_3I and $PbCl_2$ is mediated by the release of intermediate gaseous CH_3NH_3Cl (or other organic chlorides).[62-64] As a result, the Cl content in $CH_3NH_3PbI_{3-x}Cl_x$ decreases with annealing time, and the precise amount of Cl and its distribution after the complete perovskite formation sensitively depends on the processing details.[62,64] Most likely, in the presence of Zn in the ETL, the Cl evaporation takes place very quickly, causing faster crystallization of $CH_3NH_3PbI_{3-x}Cl_x$. In other words, the volatile Cl-containing compounds may react with the Zn-containing oxide ETL, which drives the reaction of perovskite formation. It will be interesting to explore if other ETLs can lead to such a fast nucleation behavior similar to ZnO and ZTO, and in-depth understanding will surely benefit the efficient and reliable synthesis of high-quality perovskite films.

4. Conclusion

In summary, we have demonstrated efficient mixed-halide perovskite solar cells with negligible hysteresis and high stability using spinal-structured ZTO as the ETL. Importantly, we found that mp-ZTO significantly accelerates the crystallization of the perovskite layers, and with simple one-step spin coating, we achieved a bilayer structure of perovskite with uniform and full surface coverage. The ultrafast transient spectroscopy study revealed fast and efficient photo-

carrier extraction by the ZTO layers from the perovskite. Fast charge transfer and good perovskite crystallization lead to negligible hysteresis in the *J-V* curves of our perovskite solar cells. The energy conversion efficiency of such ZTO-based solar cells reaches 13.34%, and it can be maintained at a level of 10% over a period of one month without any encapsulation. Overall, our results highlight ZTO as a promising ETL for unleashing the potential of stable hysteresis-free perovskite solar cells, and the strategy of interface engineering should be further exploited in future to achieve better device performance.

Acknowledgement

Research reported in this publication was supported by the King Abdullah University of Science and Technology (KAUST).

Supporting Information

BET and the optical transmittance of the mesoporous ZTO layers, Transmittance and the SEM images of the $CH_3NH_3PbI_{3-x}Cl_x$ on meso-TiO_2, and the device performance, optical photographs of $CH_3NH_3PbI_{3-x}Cl_x$. This material is available free of charge via the Internet at http:// pubs.acs.org.

References

1. Burschka, J.; Pellet, N.; Moon, S.-J.; Humphry-Baker, R.; Gao, P.; Nazeeruddin, M. K.; Graetzel, M., Sequential Deposition As A Route To High-Performance Perovskite-Sensitized Solar Cells. *Nature* **2013,** *499*, 316.

2. Leijtens, T.; Eperon, G. E.; Pathak, S.; Abate, A.; Lee, M. M.; Snaith, H. J., Overcoming Ultraviolet Light Instability Of Sensitized Tio_2 With Meso-Superstructured Organometal Tri-Halide Perovskite Solar Cells. *Nat. Commun.* **2013,** *4*, 2885.

3. Jeon, N. J.; Noh, J. H.; Kim, Y. C.; Yang, W. S.; Ryu, S.; Seok, S. I., Solvent Engineering For High-Performance Inorganic–Organic Hybrid Perovskite Solar Cells. *Nat. Mater.* **2014,** *13*, 897-903.

4. Zhou, H.; Chen, Q.; Li, G.; Luo, S.; Song, T.-b.; Duan, H.-S.; Hong, Z.; You, J.; Liu, Y.; Yang, Y., Interface Engineering Of Highly Efficient Perovskite Solar Cells. *Science* **2014,** *345*, 542-546.

5. Heo, J. H.; Im, S. H.; Noh, J. H.; Mandal, T. N.; Lim, C.-S.; Chang, J. A.; Lee, Y. H.; Kim, H.-j.; Sarkar, A.; Nazeeruddin, M. K.; Graetzel, M.; Seok, S. I., Efficient Inorganic-Organic Hybrid Heterojunction Solar Cells Containing Perovskite Compound And Polymeric Hole Conductors. *Nat. Photonics* **2013,** *7*, 487-492.

6. Stranks, S. D.; Eperon, G. E.; Grancini, G.; Menelaou, C.; Alcocer, M. J. P.; Leijtens, T.; Herz, L. M.; Petrozza, A.; Snaith, H. J., Electron-Hole Diffusion Lengths Exceeding 1 Micrometer in an Organometal Trihalide Perovskite Absorber. *Science* **2013,** *342*, 341-344.

7. Eperon, G. E.; Burlakov, V. M.; Docampo, P.; Goriely, A.; Snaith, H. J., Morphological Control for High Performance, Solution-Processed Planar Heterojunction Perovskite Solar Cells. *Adv. Func. Mater.* **2014,** *24*, 151-157.

8. Liu, M.; Johnston, M. B.; Snaith, H. J., Efficient Planar Heterojunction Perovskite Solar Cells By Vapour Deposition. *Nature* **2013,** *501*, 395.

9. Kim, H.-S.; Lee, C.-R.; Im, J.-H.; Lee, K.-B.; Moehl, T.; Marchioro, A.; Moon, S.-J.; Humphry-Baker, R.; Yum, J.-H.; Moser, J. E.; Graetzel, M.; Park, N.-G., Lead Iodide Perovskite Sensitized All-Solid-State Submicron Thin Film Mesoscopic Solar Cell with Efficiency Exceeding 9%. *Sci. Rep.* **2012,** *2*, 591.

10. Eperon, G. E.; Stranks, S. D.; Menelaou, C.; Johnston, M. B.; Herz, L. M.; Snaith, H. J., Formamidinium Lead Trihalide: A Broadly Tunable Perovskite For Efficient Planar Heterojunction Solar Cells. *Energy Environ. Sci.* **2014,** *7*, 982-988.

11. Im, J.-H.; Lee, C.-R.; Lee, J.-W.; Park, S.-W.; Park, N.-G., 6.5% Efficient Perovskite Quantum-Dot-Sensitized Solar Cell. *Nanoscale* **2011,** *3*, 4088-4093.

12. Kojima, A.; Teshima, K.; Shirai, Y.; Miyasaka, T., Organometal Halide Perovskites as Visible-Light Sensitizers for Photovoltaic Cells. *J. Am. Chem. Soc.* **2009,** *131*, 6050-6051.

13. Lee, M. M.; Teuscher, J.; Miyasaka, T.; Murakami, T. N.; Snaith, H. J., Efficient Hybrid Solar Cells Based on Meso-Superstructured Organometal Halide Perovskites. *Science* **2012,** *338*, 643-647.

14. Jiang, Q.; Sheng, X.; Shi, B.; Feng, X.; Xu, T., Nickel-Cathoded Perovskite Solar Cells. *J. Phys. Chem. C* **2014,** *118*, 25878-25883.

15. Heo, J. H.; You, M. S.; Chang, M. H.; Yin, W.; Ahn, T. K.; Lee, S.-J.; Sung, S.-J.; Kim, D. H.; Im, S. H., Hysteresis-Less Mesoscopic $CH_3NH_3PbI_3$ Perovskite Hybrid Solar Cells By Introduction Of Li-Treated Tio_2 Electrode. *Nano Energy* **2015,** *15*, 530-539.

16. Wang, X.; Li, Z.; Xu, W.; Kulkarni, S. A.; Batabyal, S. K.; Zhang, S.; Cao, A.; Wong, L. H., TiO_2 Nanotube Arrays Based Flexible Perovskite Solar Cells With Transparent Carbon Nanotube Electrode. *Nano Energy* **2015,** *11*, 728-735.

17. De Wolf, S.; Holovsky, J.; Moon, S.-J.; Löper, P.; Niesen, B.; Ledinsky, M.; Haug, F.-J.; Yum, J.-H.; Ballif, C., Organometallic Halide Perovskites: Sharp Optical Absorption Edge and Its Relation to Photovoltaic Performance. *J. Phys. Chem. Lett.* **2014,** *5*, 1035-1039.

18. Li, F.; Ma, C.; Wang, H.; Hu, W.; Yu, W.; Sheikh, A. D.; Wu, T., Ambipolar Solution-Processed Hybrid Perovskite Phototransistors. *Nature Commun.* **2015,** *6*, 8238.

19. Xing, G.; Mathews, N.; Sun, S.; Lim, S. S.; Lam, Y. M.; Graetzel, M.; Mhaisalkar, S.; Sum, T. C., Long-Range Balanced Electron- and Hole-Transport Lengths in Organic-Inorganic $CH_3NH_3PbI_3$. *Science* **2013,** *342*, 344-347.

20. Noh, J. H.; Im, S. H.; Heo, J. H.; Mandal, T. N.; Seok, S. I., Chemical Management for Colorful, Efficient, and Stable Inorganic–Organic Hybrid Nanostructured Solar Cells. *Nano Lett.* **2013,** *13*, 1764-1769.

21. Nagane, S.; Bansode, U.; Game, O.; Chhatre, S.; Ogale, S., $CH_3NH_3PbI_{(3-X)}(BF_4)_X$: Molecular Ion Substituted Hybrid Perovskite. *Chem. Commun.* **2014,** *50*, 9741-9744.

22. Docampo, P.; Ball, J. M.; Darwich, M.; Eperon, G. E.; Snaith, H. J., Efficient Organometal Trihalide Perovskite Planar-Heterojunction Solar Cells On Flexible Polymer Substrates. *Nat. Commun.* **2013,** *4*, 2761.

23. Conings, B.; Baeten, L.; De Dobbelaere, C.; D'Haen, J.; Manca, J.; Boyen, H.-G., Perovskite-Based Hybrid Solar Cells Exceeding 10% Efficiency with High Reproducibility Using a Thin Film Sandwich Approach. *Adv. Mater.* **2014,** *26*, 2041-2046.

24. Dualeh, A.; Tétreault, N.; Moehl, T.; Gao, P.; Nazeeruddin, M. K.; Grätzel, M., Effect of Annealing Temperature on Film Morphology of Organic–Inorganic Hybrid Pervoskite Solid-State Solar Cells. *Adv. Func. Mater.* **2014,** *24*, 3250-3258.

25. Leijtens, T.; Lauber, B.; Eperon, G. E.; Stranks, S. D.; Snaith, H. J., The Importance of Perovskite Pore Filling in Organometal Mixed Halide Sensitized TiO_2-Based Solar Cells. *J. Phys. Chem. Lett.* **2014,** *5*, 1096-1102.

26. Li, G.; Ching, K. L.; Ho, J. Y. L.; Wong, M.; Kwok, H.-S., Identifying the Optimum Morphology in High-Performance Perovskite Solar Cells. *Adv. Energy Mater.* **2015,** *5*, 1401775.

27. Ke, W.; Fang, G.; Wang, J.; Qin, P.; Tao, H.; Lei, H.; Liu, Q.; Dai, X.; Zhao, X., Perovskite Solar Cell with an Efficient TiO_2 Compact Film. **2014,** *6*, 15959-15965.

28. Choi, S.-H.; Hwang, D.; Kim, D.-Y.; Kervella, Y.; Maldivi, P.; Jang, S.-Y.; Demadrille, R.; Kim, I.-D., Amorphous Zinc Stannate (Zn_2SnO_4) Nanofibers Networks as Photoelectrodes for Organic Dye-Sensitized Solar Cells. *Adv. Func. Mater.* **2013,** *23*, 3146-3155.

29. Tan, B.; Toman, E.; Li, Y.; Wu, Y., Zinc Stannate (Zn_2SnO_4) Dye-Sensitized Solar Cells. *J. Am. Chem. Soc.* **2007,** *129*, 4162.

30. Oh, L. S.; Kim, D. H.; Lee, J. A.; Shin, S. S.; Lee, J.-W.; Park, I. J.; Ko, M. J.; Park, N.-G.; Pyo, S. G.; Hong, K. S.; Kim, J. Y., Zn_2SnO_4-Based Photoelectrodes for Organolead Halide Perovskite Solar Cells. *J. Phys. Chem. C* **2014,** *118*, 22991-22994.

31. Mali, S. S.; Su Shim, C.; Kook Hong, C., Highly Porous Zinc Stannate (Zn_2SnO_4) Nanofibers Scaffold Photoelectrodes For Efficient Methyl Ammonium Halide Perovskite Solar Cells. *Sci. Rep.* **2015,** *5*, 11424.

32. Shin, S. S.; Yang, W. S.; Noh, J. H.; Suk, J. H.; Jeon, N. J.; Park, J. H.; Kim, J. S.; Seong, W. M.; Seok, S. I., High-Performance Flexible Perovskite Solar Cells Exploiting Zn_2SnO_4 Prepared In Solution Below 100 °C. *Nature Commun.* **2015,** *6*, 150622.

33. Crossland, E. J.; Noel, N.; Sivaram, V.; Leijtens, T.; Alexander-Webber, J. A.; Snaith, H. J., Mesoporous Tio_2 Single Crystals Delivering Enhanced Mobility And Optoelectronic Device Performance. *Nature* **2013,** *495*, 215-219.

34. Snaith, H. J.; Abate, A.; Ball, J. M.; Eperon, G. E.; Leijtens, T.; Noel, N. K.; Stranks, S. D.; Wang, J. T.-W.; Wojciechowski, K.; Zhang, W., Anomalous Hysteresis in Perovskite Solar Cells. *J. Phys. Chem. Lett.* **2014,** *5*, 1511-1515.

35. Wu, K.; Bera, A.; Ma, C.; Du, Y.; Yang, Y.; Li, L.; Wu, T., Temperature-Dependent Excitonic Photoluminescence Of Hybrid Organometal Halide Perovskite Films. *Phys. Chem. Chem. Phys.* **2014,** *16*, 22476-22481.

36. Sheikh, A. D.; Bera, A.; Haque, M. A.; Rakhi, R. B.; Gobbo, S. D.; Alshareef, H. N.; Wu, T., Atmospheric Effects On The Photovoltaic Performance Of Hybrid Perovskite Solar Cells. *Sol. Energy Mater. Sol. Cells* **2015,** *137*, 6-14.

37. Di Giacomo, F.; Razza, S.; Matteocci, F.; D'Epifanio, A.; Licoccia, S.; Brown, T. M.; Di Carlo, A., High Efficiency $CH_3NH_3PbI_{(3-x)}Cl_x$ Perovskite Solar Cells With Poly(3-hexylthiophene) Hole Transport Layer. *J. Power Sources* **2014,** *251*, 152-156.

38. Jeong, S.; Jeong, Y.; Moon, J., Solution-Processed Zinc Tin Oxide Semiconductor for Thin-Film Transistors. *J. Phys. Chem. C* **2008,** *112*, 11082-11085.

39. Alpuche-Aviles, M. A.; Wu, Y., Photoelectrochemical Study of the Band Structure of Zn2SnO4 Prepared by the Hydrothermal Method. *J. Am. Chem. Soc.* **2009,** *131*, 3216-3224.

40. Jackson, W. B.; Hoffman, R. L.; Herman, G. S., High-Performance Flexible Zinc Tin Oxide Field-Effect Transistors. *Appl. Phys. Lett.* **2005,** *87*, 193503.

41. Coutts, T. J.; Young, D. L.; Li, X.; Mulligan, W. P.; Wu, X., Search For Improved Transparent Conducting Oxides: A Fundamental Investigation Of Cdo, Cd_2SnO_4, And Zn_2SnO_4. *J. Vac. Sci. Technol. A* **2000,** *18*, 2646-2660.

42. Zhang, Q.; Dandeneau, C. S.; Zhou, X.; Cao, G., ZnO Nanostructures for Dye-Sensitized Solar Cells. *Adv. Mater.* **2009,** *21*, 4087-4108.

43. Shin, S. S.; Kim, D. W.; Hwang, D.; Suk, J. H.; Oh, L. S.; Han, B. S.; Kim, D. H.; Kim, J. S.; Kim, D.; Kim, J. Y.; Hong, K. S., Controlled Interfacial Electron Dynamics in Highly Efficient Zn2SnO4-Based Dye-Sensitized Solar Cells. *Chem. Sus. Chem.* **2014,** *7*, 501-509.

44. Schwartz, R. W.; Clem, P. G.; Voigt, J. A.; Byhoff, E. R.; Van Stry, M.; Headley, T. J.; Missert, N. A., Control of Microstructure and Orientation in Solution-Deposited $BaTiO_3$ and $SrTiO_3$ Thin Films. *J. Am. Ceram. Soc.* **1999,** *82*, 2359-2367.

45. Bera, A.; Wu, K.; Sheikh, A.; Alarousu, E.; Mohammed, O. F.; Wu, T., Perovskite Oxide $SrTiO_3$ as an Efficient Electron Transporter for Hybrid Perovskite Solar Cells. *J. Phys. Chem. C* **2014,** *118*, 28494-28501.

46. Chen, Z.; Li, H.; Tang, Y.; Huang, X.; Ho, D.; Lee, C.-S., Shape-Controlled Synthesis Of Organolead Halide Perovskite Nanocrystals And Their Tunable Optical Absorption. *Mater. Res. Exp.* **2014,** *1*, 039501.

47. Stoumpos, C. C.; Malliakas, C. D.; Kanatzidis, M. G., Semiconducting Tin and Lead Iodide Perovskites with Organic Cations: Phase Transitions, High Mobilities, and Near-Infrared Photoluminescent Properties. *Inorg. Chem.* **2013,** *52*, 9019-9038.

48. Unger, E. L.; Bowring, A. R.; Tassone, C. J.; Pool, V. L.; Gold-Parker, A.; Cheacharoen, R.; Stone, K. H.; Hoke, E. T.; Toney, M. F.; McGehee, M. D., Chloride in Lead Chloride-Derived Organo-Metal Halides for Perovskite-Absorber Solar Cells. *Chem. Mater.* **2014,** *26*, 7158-7165.

49. Song, T.-B.; Chen, Q.; Zhou, H.; Luo, S.; Yang, Y.; You, J.; Yang, Y., Unraveling Film Transformations And Device Performance Of Planar Perovskite Solar Cells. *Nano Energy* **2015,** *12*, 494-500.

50. Kim, H.-S.; Park, N.-G., Parameters AffectingI–VHysteresis of CH3NH3PbI3Perovskite Solar Cells: Effects of Perovskite Crystal Size and Mesoporous TiO_2 Layer. *J. Phys. Chem. Lett.* **2014,** *5*, 2927-2934.

51. Unger, E. L.; Hoke, E. T.; Bailie, C. D.; Nguyen, W. H.; Bowring, A. R.; Heumuller, T.; Christoforo, M. G.; McGehee, M. D., Hysteresis and Transient Behavior in Current-Voltage Measurements of Hybrid-Perovskite Absorber Solar Cells. *Energy Environ. Sci.* **2014,** *7*, 3690-3698.

52. Manser, J. S.; Kamat, P. V., Band Filling with Free Charge Carriers in Organometal Halide Perovskites. *Nat. Photon.* **2014,** *8*, 737-743.

53. Zhu, Z.; Ma, J.; Wang, Z.; Mu, C.; Fan, Z.; Du, L.; Bai, Y.; Fan, L.; Yan, H.; Phillips, D. L.; Yang, S., Efficiency Enhancement of Perovskite Solar Cells through Fast Electron Extraction: The Role of Graphene Quantum Dots. *J. Am. Chem. Soc.* **2014,** *136*, 3760-3763.

54. Aly, S. M.; Ahmed, G. H.; Shaheen, B. S.; Sun, J.; Mohammed, O. F., Molecular-Structure Control of Ultrafast Electron Injection at Cationic Porphyrin–CdTe Quantum Dot Interfaces. *J. Phys. Chem. Lett.* **2015,** *6,* 791-795.

55. Mohammed, O. F.; Xiao, D.; Batista, V. S.; Nibbering, E. T. J., Excited-State Intramolecular Hydrogen Transfer (ESIHT) of 1,8-Dihydroxy-9,10-anthraquinone (DHAQ) Characterized by Ultrafast Electronic and Vibrational Spectroscopy and Computational Modeling. *J. Phys. Chem. A* **2014,** *118,* 3090-3099.

56. Christians, J. A.; Fung, R. C. M.; Kamat, P. V., An Inorganic Hole Conductor for Organo-Lead Halide Perovskite Solar Cells. Improved Hole Conductivity with Copper Iodide. *J. Am. Chem. Soc.* **2013,** *136*, 758-764.

57. Abate, A.; Leijtens, T.; Pathak, S.; Teuscher, J.; Avolio, R.; Errico, M.E.; Kirkpatrik. J.; Ball, J.M.; Docampo, P., McPherson, I.; Snaith, H.J., Lithium Salts As "Redox Active" P-Type Dopants For Organic Semiconductors And Their Impact In Solid-State Dye-Sensitized Solar Cells, *Phys. Chem. Chem. Phys.* **2013,** *15,* 2572–2579.

58. Wang, H.; Xu, M.; Liu, G.; Li, X.; Xiang, P.; Ku, Z.; Rong, Y.; Liu, L.; Hu, M.; Yang, Y.; Han, H., Effect Of Photo-Doping On Performance For Solid-State Dye-Sensitized Solar Cell Based On 2,20 -7,70 -Tetrakis-(N,N-Di-P-Methoxyphenylamine)-9,9- Spirobifluorene And Carbon Counter Electrode. *Electrochim. Acta* **2013,** *99,* 238–241.

59. Nie, W.; Tsai, H.; Asadpour, R.; Blancon, J.-C.; Neukirch, A. J.; Gupta, G.; Crochet, J. J.; Chhowalla, M.; Tretiak, S.; Alam, M. A.; Wang, H.-L.; Mohite, A. D., High-Efficiency Solution-Processed Perovskite Solar Cells With Millimeter-Scale Grains. *Science* **2015,** *347*, 522-525.

60. Yun, J. S.; Ho-Baillie, A.; Huang, S.; Woo, S. H.; Heo, Y.; Seidel, J.; Huang, F.; Cheng, Y.-B.; Green, M. A., Benefit of Grain Boundaries in Organic–Inorganic Halide Planar Perovskite Solar Cells. *J. Phys. Chem. Lett.* **2015,** *6*, 875-880.

61 Zhang, J.; Juarez-Perez, E. J.; Mora-Sero, I.; Viana, B.; Pauporte, T., Fast and Low Temperature Growth of Electron Transport Layers for Efficient Perovskite Solar Cells. *J Mater. Chem. A* **2015,** *3,* 4909–4915.

62. Unger, E. L.; Bowring, A. R.; Tassone, C. J.; Pool, V. L.; Gold-Parker, A.; Cheacharoen, R.; Stone, K. H.; Hoke, E. T.; Toney, M. F.; and McGehee, M. D., Chloride in Lead Chloride-Derived Organo-Metal Halides for Perovskite-Absorber Solar Cells. *Chem. Mater.* **2014,** *26,* 7158–7165.

63. Williams, S. T.; Zuo, F.; Chueh, C. C.; Liao, C. Y.; Liang, P. W.; and A. K. Y. Jen, Role of Chloride in the Morphological Evolution of Organo-Lead Halide Perovskite Thin Films *ACS Nano,* **2014,** *8,* 10640–10654.

64. Yu, H.; Wang, F.; Xie, F.; Li, W.; Chen, J.; and Zhao, N., The Role of Chlorine in the Formation Process of "$CH_3NH_3PbI_{3-x}Cl_x$" Perovskite, *Adv. Funct. Mater.* 201424, 7102–7108.

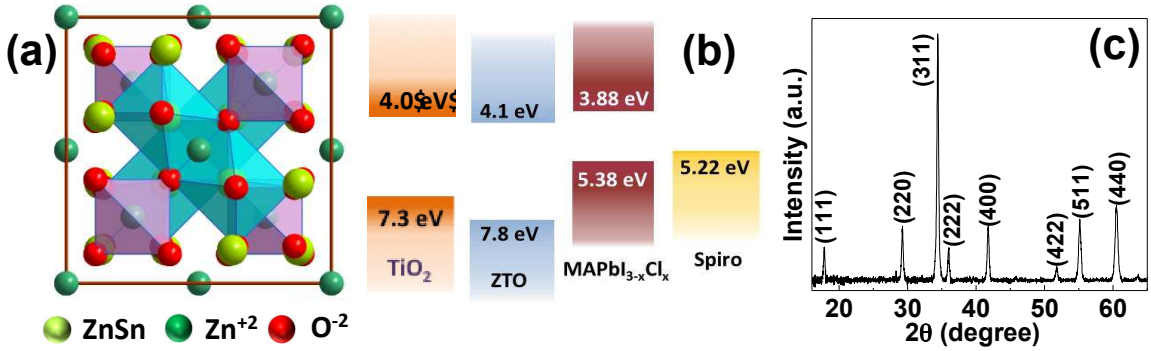

Figure 1. (a) Crystal structure of the cubic spinel-structured ZTO. (b) Schematic of the band alignment between ZTO, $CH_3NH_3PbI_{3-X}Cl_x$, and spiro-MeOTAD in the perovskite solar cell. The band structure of TiO_2 is also added for comparison. (c) XRD pattern of the mp-ZTO layer.

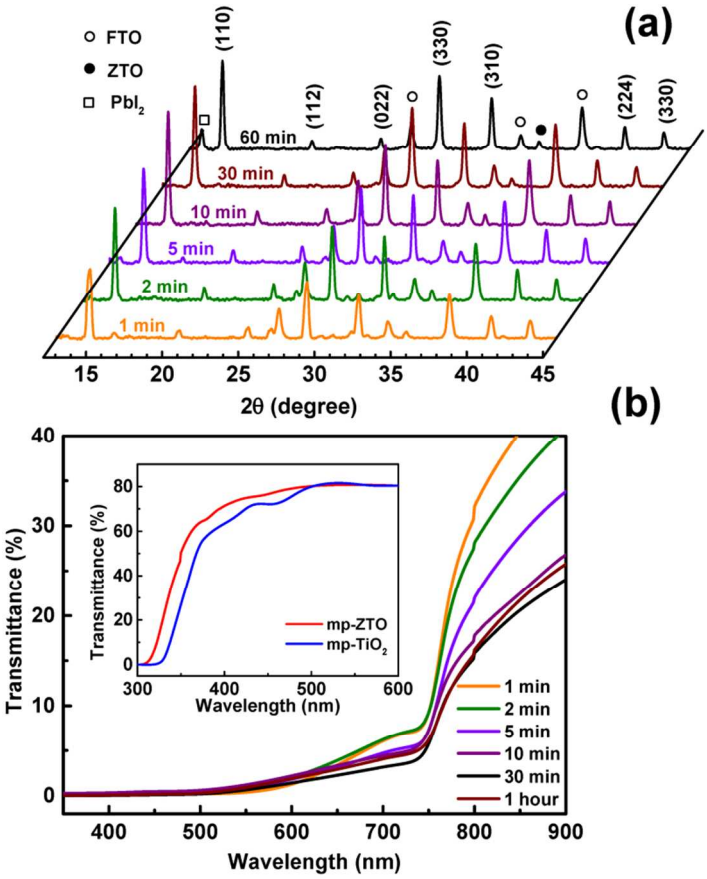

Figure 2. Evolution of crystallization and structure of the perovskite film on ZTO during annealing at 100 °C: (a) XRD patterns and (b) transmission spectra. Inset of (b) presents the transmittance spectra of mp-ZTO and mp-TiO_2 layers.

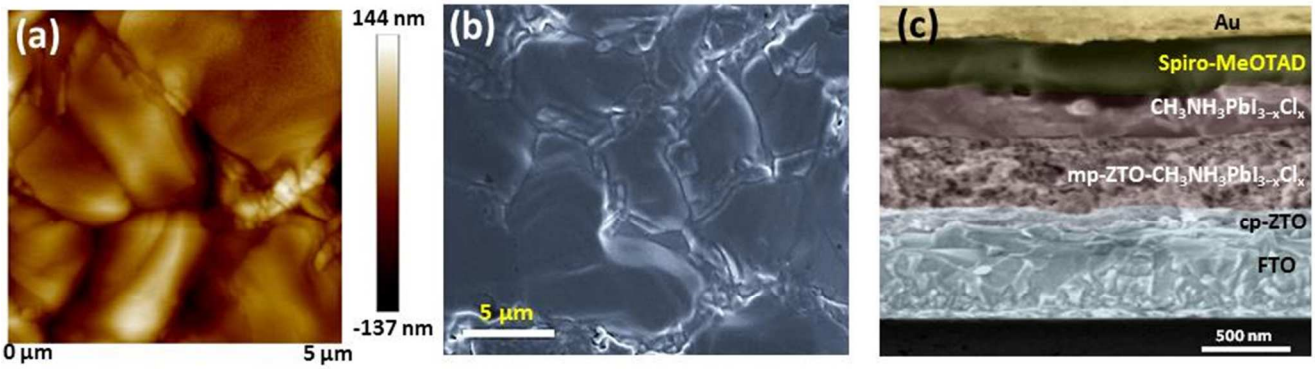

Figure 3. Surface morphology of the $CH_3NH_3PbI_{3-x}Cl_x$ layers on mp-ZTO after annealing at 100 °C for 30 minutes: (a) tapping-mode AFM height image (5 × 5 µm) and (b) top-view SEM image. (c) Cross-sectional view of the perovskite solar cell device with ZTO as ETL.

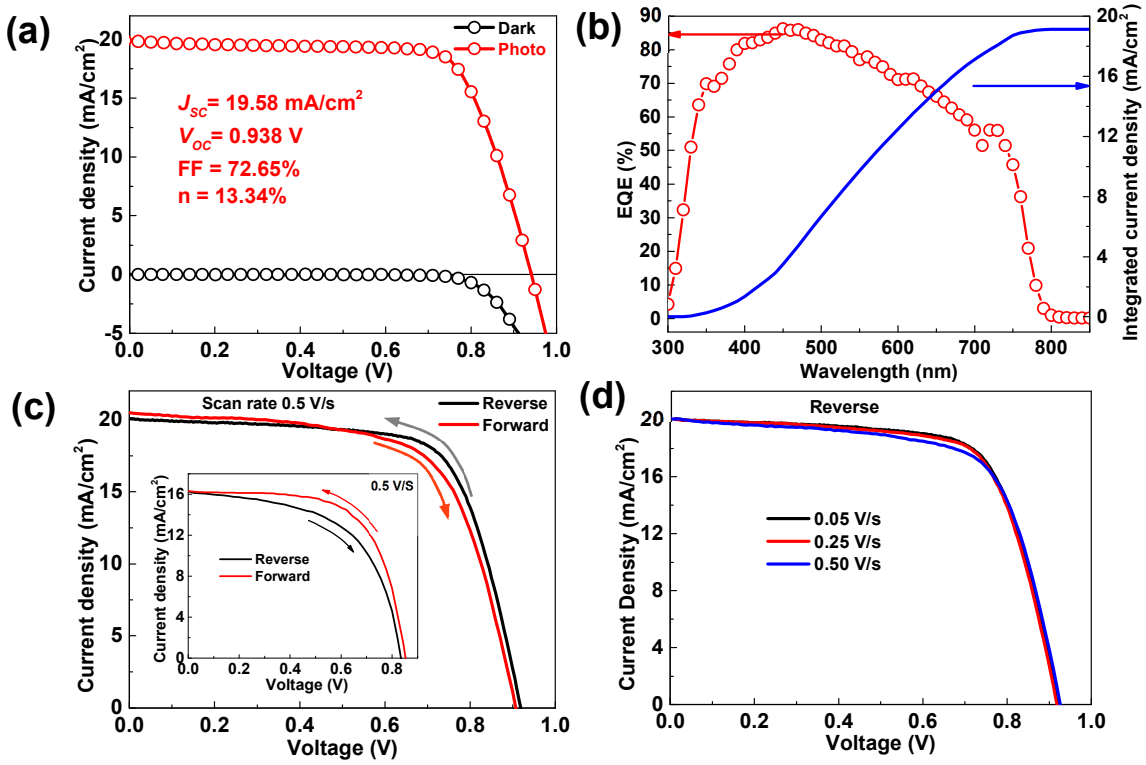

Figure 4. (a) *J-V* curves of the perovskite solar cell with ZTO ETL measured in dark and under illumination. (b) EQE spectrum and the corresponding integrated current density of the same solar cell. (c) *J-V* curves of the perovskite solar cell with the ZTO ETL measured in forward and reverse voltage scanning directions. Inset shows the typical hysteresis behavior of the *J-V* curves of the perovskite solar cell with the mp-TiO_2 ETL. (d) Scan rate dependence of the *J-V* characteristics of the perovskite solar cell with the ZTO ETL.

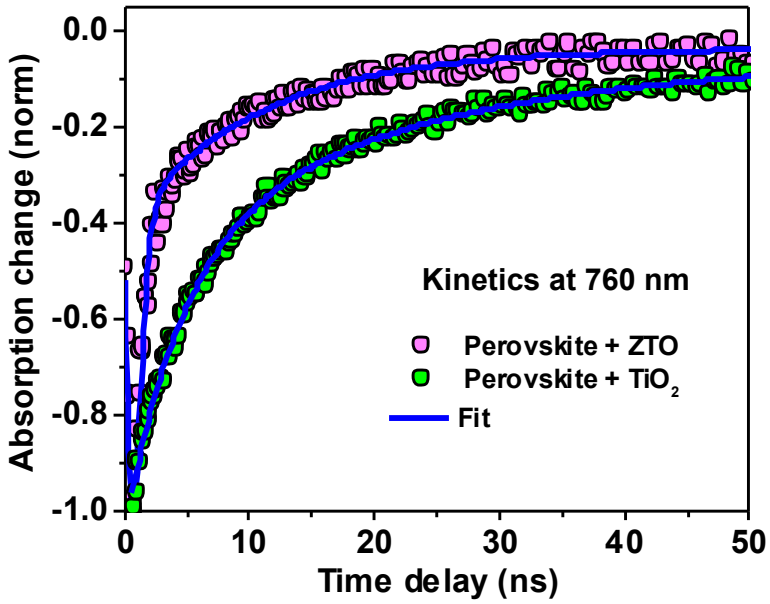

Figure 5. Normalized profiles of transient absorption for bilayers of $CH_3NH_3PbI_{3-x}Cl_x$ with ZTO and TiO_2 ETLs measured at 440 nm excitation (1 kHz, 35 fs, 1.5 μJ/cm^2).

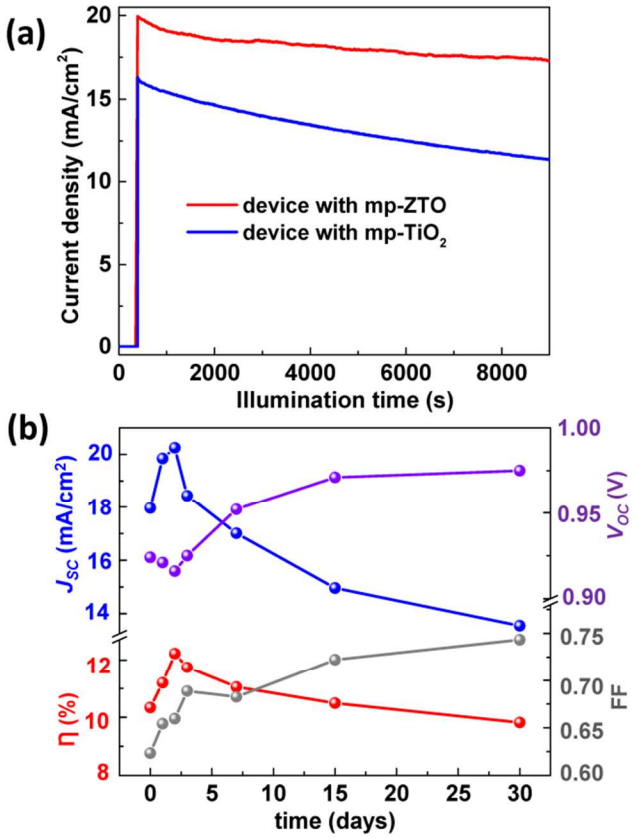

Figure 6. (a) Time dependence of J_{SC} upon continuous AM 1.5 illumination measured on perovskite solar cells without encapsulation. (b) Variations of the photovoltaic parameters as a function of storage time in ambient atmosphere for the perovskite solar cell with ZTO ETL.

TOC

Fast Crystallization and improved Stability of Perovskite Solar Cells with Zn_2SnO_4 Electron Transporting Layer: Interface Matters

*Ashok Bera[†], Arif D. Sheikh[†], Md. Azimul Haque[†], Riya Bose[I], Erkki Alarousu[I], Omar F. Mohammed[I], Tom Wu[†]**

[†]Materials Science and Engineering, King Abdullah University of Science and Technology, Thuwal, 23955-6900, Saudi Arabia.
E-mail: tao.wu@kaust.edu.sa

[I]Solar and Photovoltaics Engineering Research Center, Division of Physical Science and Engineering, King Abdullah University of Science and Technology (KAUST), Thuwal, 23955-6900, Kingdom of Saudi Arabia